Article

Low-Pb High-Piezoelectric Ceramic System $(1-x)Ba(Zr_{0.18}Ti_{0.82})O_3-x(Ba_{0.78}Pb_{0.22})TiO_3$

Chao Zhou *, Jiajing Li, Xiaoxiao Zhang, Tiantian Yu, Yin Zhang and Sen Yang *

MOE Key Laboratory for Nonequilibrium Synthesis and Modulation of Condensed Matter, School of Physics, Xi'an Jiaotong University, Xi'an 710049, China; liag120@stu.xjtu.edu.cn (J.L.); zhangxiaoxiao@stu.xjtu.edu.cn (X.Z.); ytt19980807@stu.xjtu.edu.cn (T.Y.); yzhang18@xjtu.edu.cn (Y.Z.)
* Correspondence: chao.zhou@xjtu.edu.cn (C.Z.); yang.sen@xjtu.edu.cn (S.Y.)

Abstract: Piezoelectric materials, especially Pb-based piezoelectric materials, are widely used in the key components of sensors, actuators, and transducers. Due to the rising concern of the toxicity of Pb, global legislation has been adopted to restrict the use of Pb. Given that the available Pb-free piezoelectric materials cannot replace the Pb-based ones for various reasons, we designed and fabricated a low-Pb piezoelectric solid-solution ceramic system, $(1-x)Ba(Zr_{0.18}Ti_{0.82})O_3-x(Ba_{0.78}Pb_{0.22})TiO_3$ (denoted as $BZ_{0.18}T-xBP_{0.22}T$ herein). The crystal structure, ferroelectric, dielectric, and piezoelectric properties of the $BZ_{0.18}T-xBP_{0.22}T$ system were systematically studied. With the increase in $BP_{0.22}T$ content, the structure of the samples changed from a rhombohedral phase to a tetragonal phase; the intermediate composition $x = 0.5$ was located at the morphotropic phase boundary of the system and corresponded to the state with the coexistence of the rhombohedral and tetragonal phases. Moreover, $x = 0.5$ exhibited the optimum comprehensive properties among all the samples, with a piezoelectric coefficient d_{33} of 240 pC/N, a maximum dielectric temperature Tm of 121.1°C, and a maximum polarization Pm of 15 μC/cm². Our work verifies the validity of the route to design low-Pb high-piezoelectric materials and may stimulate the interests for exploring new low-Pb high-performance ferroelectric and piezoelectric materials.

Keywords: low-Pb; piezoelectric; morphotropic phase boundary; phase transition

1. Introduction

Piezoelectric materials can realize the conversion between elastic energy and electric energy; thus, they are widely used in actuators, sensors, and transducers [1]. Since the discovery of high piezoelectricity in $Pb(Zr_{0.52}Ti_{0.48})O_3$ (PZT) [2], Pb-based piezoelectric materials, i.e., $Pb(Mg_{1/3}Nb_{2/3})O_3-PbTiO_3$ (PMN-PT) [3] and $Pb(Zn_{1/3}Nb_{2/3})O_3-PbTiO_3$ (PZN-PT) [4], have accounted for the majority of the market share [5].

However, with the rising concern regarding the hazards for both human health and the environment caused by the toxic element Pb, the use of Pb in electronic devices is facing fierce circumstance and will be rigidly limited by laws and regulations, such as "Waste Electrical and Electronic Equipment" (WEEE) and "The Restriction of the use of certain Hazardous substances in Electrical and Electronic Equipment" (RoHS). In such a situation, high-performance Pb-free or low-Pb piezoelectric materials are highly desired. In the last two decades, many Pb-free piezoelectric materials have been introduced, such as $(K_{0.5}Na_{0.5})NbO_3$ (KNN) [6], $(Bi_{1/2}Na_{1/2})TiO_3-BaTiO_3$ (BNT-BT) [7], $Ba(Zr_{0.2}Ti_{0.8})O_3-x(Ba_{0.7}Ca_{0.3})TiO_3$ (BZTBCT) [8], etc. Although much effort has been devoted to this task, it has to be admitted that all of the above-mentioned Pb-free materials face various problems; for example, the raw materials (K_2CO_3, Na_2CO_3) used to fabricate KNN are moisture-sensitive [9], the piezoelectricity of BNT-BT is inferior to most Pb-based materials [10], and the maximum dielectric temperature (Tm) is below 100°C (Tm of the optimum composition BZT-0.5BCT is 93°C) [8]. As a result, none of the above Pb-free materials can substitute for Pb-based ones.

Therefore, in the present study, we explore low-Pb high-piezoelectric materials as an alternative. As a comprehensive consideration, such a strategy will not only help people confront the situation of the strict limits on the use of Pb, it will also gain time for the exploration of Pb-free high-performance piezoelectric materials that can completely replace the Pb-based ones.

It has been well acknowledged that the design of morphotropic phase boundary (MPB) is an effective route to obtain high piezoelectricity [11]. At MPB, the coexistence of rhombohedral (*R*) and tetragonal (*T*) phases leads to the facilitated rotation and switching of polarization under external stress, thus yielding a high piezoelectric response [8,12]. The end members of such systems should meet the following criteria: (1) one end member undergoes the transition from the cubic (*C*) to *T* phase, while the other end member undergoes the transition from the *C* to *R* phase; (2) the two end members can form a solid-solution compound; then, a triple-point would exist [13]. We discovered that Zr-doped $BaTiO_3$ [14] and Pb-doped $BaTiO_3$ [15], satisfy the above requirements.

For the end member Zr-doped $BaTiO_3$, i.e., $Ba(Zr_mTi_{1-m})O_3$ (BZT), to ensure it satisfies the abovementioned criteria, m was fixed as 0.18. For the end member Pb-doped $BaTiO_3$, i.e., $(Ba_{1-n}Pb_n)TiO_3$ (BPT), the value of n should guarantee that the BPT undergoes one single transition from a cubic to a tetragonal phase. According to the phase diagram [15], when n exceeds 0.2, this occurs. Therefore, the value of n that satisfies the criterion is not unique and was selected as 0.22 in the present study. However, the value of n should not be too large, which would be contrary to our aim—"low Pb" content. Thus, based on the two end member compounds, we designed the low-Pb solid-solution system $(1-x)Ba(Zr_{0.18}Ti_{0.82})O_3-x(Ba_{0.78}Pb_{0.22})TiO_3$.

2. Materials and Methods

The $(1-x)Ba(Zr_{0.18}Ti_{0.82})O_3-x(Ba_{0.78}Pb_{0.22})TiO_3$ (denoted as $BZ_{0.18}T-xBP_{0.22}T$ hereafter; x represents the mole fraction of $(Ba_{0.78}Pb_{0.22})TiO_3$) ceramic samples were prepared with the conventional solid-state reaction method, with the raw chemicals of $BaCO_3$ (99.95%), ZrO_2 (98%), TiO_2 (99.9%), and PbO (99.9%). Considering that a Pb-induced nonstoichiometric compound usually leads to the formation of an oxygen vacancy [16], excess PbO (5 at%) was added to compensate for the loss of Pb. The calcining was performed at 1200°C in air for 2 h, and the sintering was performed at 1250°C in air for 3 h. The crystal structure was detected using an X-ray diffractometer (XRD, Bruker D8 ADVANCE, Hamburg, Germany). The temperature spectrum of dielectric permittivity was measured using an LCR meter (HIOKI-3532) at 10 kHz in a temperature chamber (Linkam), with the ramp rate of 2°C/min. The ferroelectric properties (Polarization-Electric field loops) were measured using a ferroelectric tester (Radiant Workstation Premier II, Albuquerque, NM, USA) at a frequency of 10 Hz at room temperature (22°C). The piezoelectric coefficient d_{33} was measured using a Berlincourt-type d_{33} meter (ZJ-3A). Before piezoelectric measurements, the ceramic samples were poled at 22°C for 1.5 h under an electric field of 1.0 kV/mm.

3. Results and Discussion

3.1. Structural Characterization

Figure 1a shows the X-ray diffraction (XRD) patterns for all the $BZ_{0.18}T-xBP_{0.22}T$ samples. No reflections of a second phase appeared, demonstrating that all the samples possessed a pure perovskite ABO_3 structure [17]. The XRD profile of (200) reflection is shown in Figure 1b. From x = 0 to 0.3, with the increase in $BP_{0.22}T$ content, the reflection of (200) moved toward a higher angle, revealing the lattice constant decreased, which was caused by the smaller ionic radius of Pb^{2+} [15]. No splitting of the (200) reflection suggested a rhombohedral crystal structure [17]. On the other hand, the (200) reflection moving toward a higher angle also implied that the $BZ_{0.18}T$ and $BP_{0.22}T$ formed into solid-solution; otherwise, the $BP_{0.22}T$ would distribute mainly at the grain boundary and would not change the lattice parameters [18]. From x = 0.6 to 1.0, the reflection of the (200) split into two peaks, agreeing well with the detected tetragonal crystal structure in Pb-doped

$BaTiO_3$ [15]. By contrast, the intermediate composition, x = 0.5, corresponded to the state with the coexistence of *R* and *T* phases, coined the MPB composition [8].
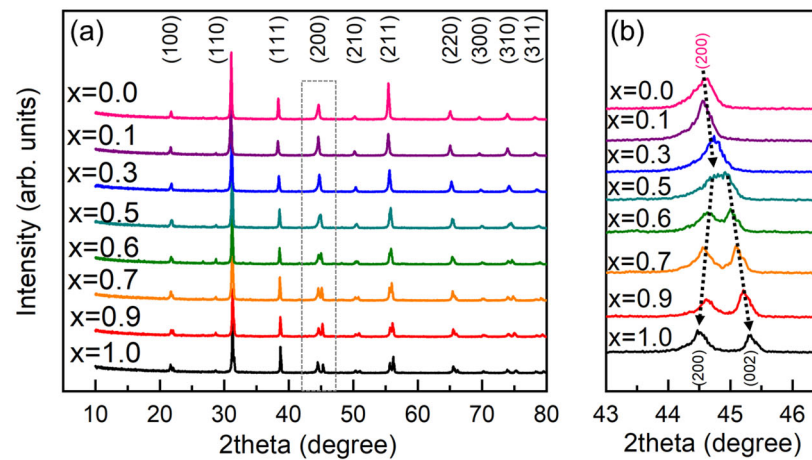

Figure 1. XRD profiles (**a**) and the (200) reflections (**b**) of the $BZ_{0.18}T–xBP_{0.22}T$ ceramic powder samples at room temperature (22°C).

3.2. Dielectric Permittivity versus Temperature Spectrum

Based on the XRD results in Figure 1, several typical compositions were selected for further investigation, x = 0, 0.1, 0.5, and 0.7. Figure 2 shows the temperature spectrum of the dielectric permittivity (ε at 10kHz) for the selected typical compositions (for ε measured at multiple frequencies, please refer to Figures S1–S4). For x = 0.0 ($BZ_{0.18}T$), which exhibited an *R* phase at room temperature, there appeared only one dielectric peak at 56.6°C, indicating the transition from the *C* to *R* phase and agreed well with a previous report [14]; for x = 0.7, which exhibited a *T* phase at room temperature, there also appeared only one peak indicating the transition from the *C* to *T* phase [15]. For the intermediate compositions x = 0.1 and x = 0.5, there appeared two dielectric peaks, of which the one at a higher temperature indicated the *C-T* transition, and the other one at a lower temperature indicated the *T-R* transition. The doped $BP_{0.22}T$ increased both the maximum dielectric temperature (Tm) and the *T-R* transition temperature. Compared with the other compositions, x = 0.5 possessed both relatively large dielectric permittivity and good temperature stability. The observed composition-dependent dielectric behavior was consistent with those of the previously reported ferroelectric MPB systems, i.e., BZT-BCT [8] and BHT-BCT [13].
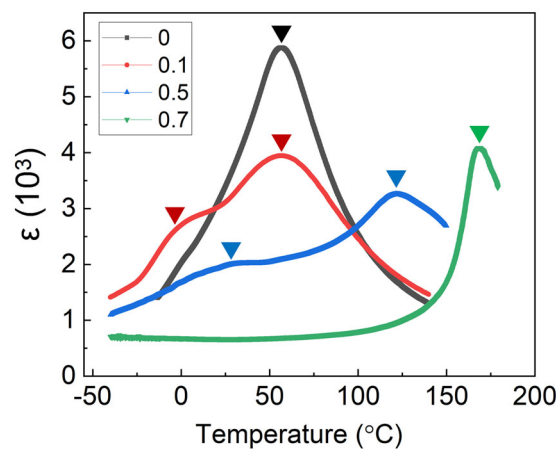

Figure 2. Dielectric permittivity versus temperature curves (10 kHz) for the selected compositions x = 0, 0.1, 0.5, and 0.7 of $BZ_{0.18}T–xBP_{0.22}T$.

Compared with a normal paraelectric–ferroelectric transition [15], the shapes of the dielectric peak at Tm for the $BZ_{0.18}T–xBP_{0.22}T$ samples expanded to a broader temperature

range, and this is the typical feature of a diffuse phase transition [19]. In the paraelectric phase, the inverse dielectric permittivity ($1/\varepsilon$) for ferroelectric materials obeys the Curie–Weiss Law [19]:

$$\frac{1}{\varepsilon} = \frac{T - T_C}{C} \tag{1}$$

where T_C is the Curie temperature, and C is the Curie–Weiss constant.

The inverse dielectric permittivity versus temperature curves of the typical compositions x = 0, 0.1, 0.5, and 0.7 are depicted in Figure 3. To investigate the diffuse phase transition behaviors of the $BZ_{0.18}T–xBP_{0.22}T$ samples, the modified Curie–Weiss Law was employed [20]:

$$\frac{1}{\varepsilon} - \frac{1}{\varepsilon_m} = \frac{(T - T_m)^\gamma}{C} \tag{2}$$

where γ denotes the degree of diffusion constant; $\gamma = 1$ indicates the normal ferroelectric transition behavior, and $\gamma = 2$ indicates the complete diffuse phase transition behavior, commonly regarded as relaxor behavior [19].
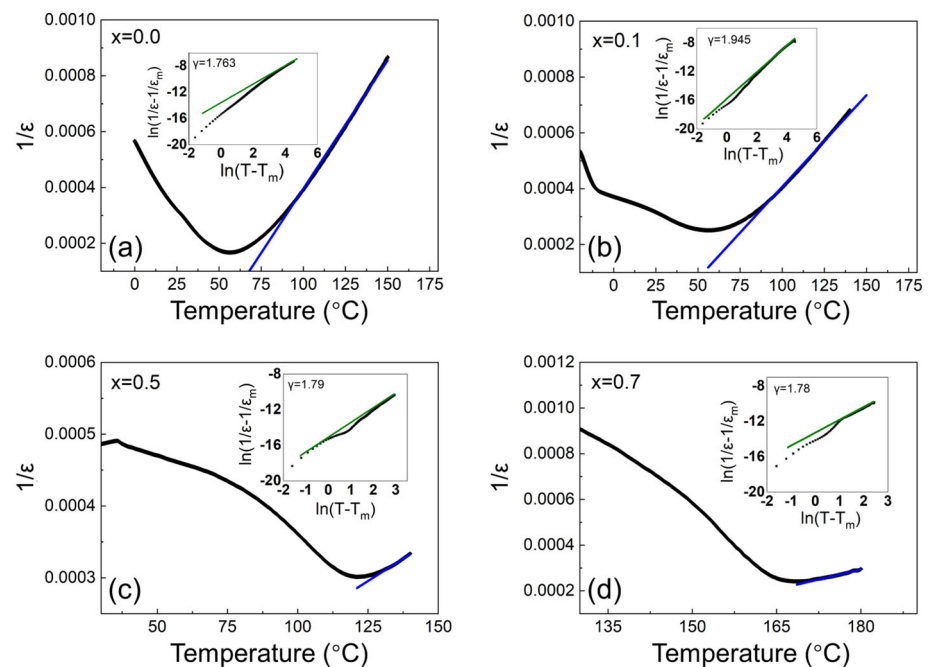

Figure 3. The inverse dielectric permittivity (10 kHz) versus temperature curves and corresponding fitted $\ln(\frac{1}{\varepsilon} - \frac{1}{\varepsilon_m})$ versus $\ln(T - T_m)$ curves (inset) for the selected compositions x = 0 (**a**), 0.1 (**b**), 0.5 (**c**), and 0.7 (**d**) of $BZ_{0.18}T–xBP_{0.22}T$. The blue lines denote the linear fitting of $1/\varepsilon\sim T$ above T_C, and the green lines denote the linear fitting of $\ln(\frac{1}{\varepsilon} - \frac{1}{\varepsilon_m}) \sim \ln(T - T_m)$ at high temperature regime.

The plots of $\ln(\frac{1}{\varepsilon} - \frac{1}{\varepsilon_m})$ versus $\ln(T - T_m)$ curves are shown in the insets of Figure 3. The fitted parameters, T_C, T_m, and C and the estimated values of γ for x = 0, 0.1, 0.5, and 0.7 are listed in Table 1.

The composition x = 0.1 exhibited the strongest diffuse phase transition behavior, which can be understood from two aspects: (1) on one hand, as can be seen in Figure 2, the transition peak corresponded to the convergence of the *C-T* and *T-R* transitions; (2) on the other hand, for the solid-solution system (1−x)BZT–xBPT, while the content of the BPT was low (i.e., 0 < x ≤ 0.1), the solution can be regarded as Pb and Ti co-doped BZT. Although Pb^{2+} and Ba^{2+} are of equal valence, their ionic radii are different. Substitution of Zr^{4+} with Ti^{4+} is of the same type. Therefore, co-doping of Pb^{2+} and Ti^{4+} would probably result in a relaxor-like state [21].

Table 1. The dielectric parameters of $BZ_{0.18}T–xBP_{0.22}T$ (x = 0.0, 0.1, 0.5, 0.7) at 10 kHz.

Composition	T_C (°C)	T_m (°C)	C (°C)	γ
0.0	48.8	56.4	3.63×10^6	1.763
0.1	54.6	56.0	1.14×10^7	1.945
0.5	85.0	121.1	6.10×10^6	1.790
0.7	130.0	168.6	1.21×10^6	1.780

It should be noted that the Tm of the MPB composition of the $BZ_{0.18}T–xBP_{0.22}T$ system, x = 0.5, was 121.1°C, nearly thirty degrees higher than that of the famous MPB composition BZT-0.5BCT (93°C) [8]. This means that the upper limit of working temperature for $BZ_{0.18}T$-$0.5BP_{0.22}T$ is higher than that of BZT-0.5BCT, proving the validity of designing low-Pb high-piezoelectric materials via the MPB mechanism.

3.3. Ferroelectric and Piezoelectric Properties

The polarization (P)—ferroelectric field (E) hysteresis loops are shown in Figure 4. With the increase in $BP_{0.22}T$ content from x = 0 to x = 0.5, the maximum polarization Pm and remnant polarization Pr first increased and then decreased, both reaching the maximum value at x = 0.5, which is clearly seen in Figure 5a,b, respectively. Generally, the enhancement of polarization results mainly from two factors: (1) the increase in the intrinsic spontaneous polarization [22] and (2) the facilitation of the ferroelectric domain switching [23]. As for the $BZ_{0.18}T–xBP_{0.22}T$ system, both factors may contribute to the observed increase in polarization. On one hand, the increasing content of $BP_{0.22}T$ is essentially equal to the increasing substitution of $BaTiO_3$ by $PbTiO_3$. $PbTiO_3$ possesses a larger c/a ratio, which results in a larger ionic polarization [24]; so the introduction of $BP_{0.22}T$ (within a certain amount) leads to the increase in intrinsic spontaneous polarization [15]. On the other hand, when the volume fraction of $BP_{0.22}T$ reaches a certain content, as 50 at% (x = 0.5) in the present study, the material locates at the MPB that corresponds to the state where the *R* phase and *T* phase coexist. The thermodynamic state at MPB has been well illustrated as the flattening of the Landau energy landscape with near-zero energy barrier between different neighboring phases [25,26]. At MPB, the ferroelectric domain can be switched under a lower field (although the coercive field E_C of x = 0.5 was not the minimum among all the compositions) [12]. Therefore, the maximum polarization was obtained at x = 0.5. From x = 0.5 to 1.0, the greater potential well depths of $PbTiO_3$ gradually dominated and caused the domain switching to become more difficult as evidenced by the changing trend of E_C (Figure 5c) [27]; so, the polarization decreased monotonously as the content increased from x = 0.5 to 1.0.

As for the minimum E_C appearing at x = 0.3, it was probably due to the observed "invisible phase boundary" in such MPB-involved systems [28]. For the triple-point MPB involved system, the MPB derives from its starting point—the triple-point where three phases coexist [13]. Such phase coexistence naturally gives rise to the minimum energy barrier within the whole diagram; so, the MPB that derives from it yields a large response under small external fields. The minimum E_C appearing at x = 0.3 suggested that the triple point of the system corresponded to the composition x = 0.3, similar to a previously reported $(1-x)Ba(Ti_{0.8}Hf_{0.2})O_3–x(Ba_{0.7}Ca_{0.3})TiO_3$ system [28,29]. In addition, from x = 0.3 to 1.0, E_C increased monotonously; this phenomenon was ascribed to the abovementioned greater potential well depths of $PbTiO_3$ [30].This could also explain the difference between the $BZ_{0.18}T–xBP_{0.22}T$ system and the BZT-BCT system; for the BZT-BCT, the lowest E_C was observed at the MPB composition BZT-0.5BCT [8].
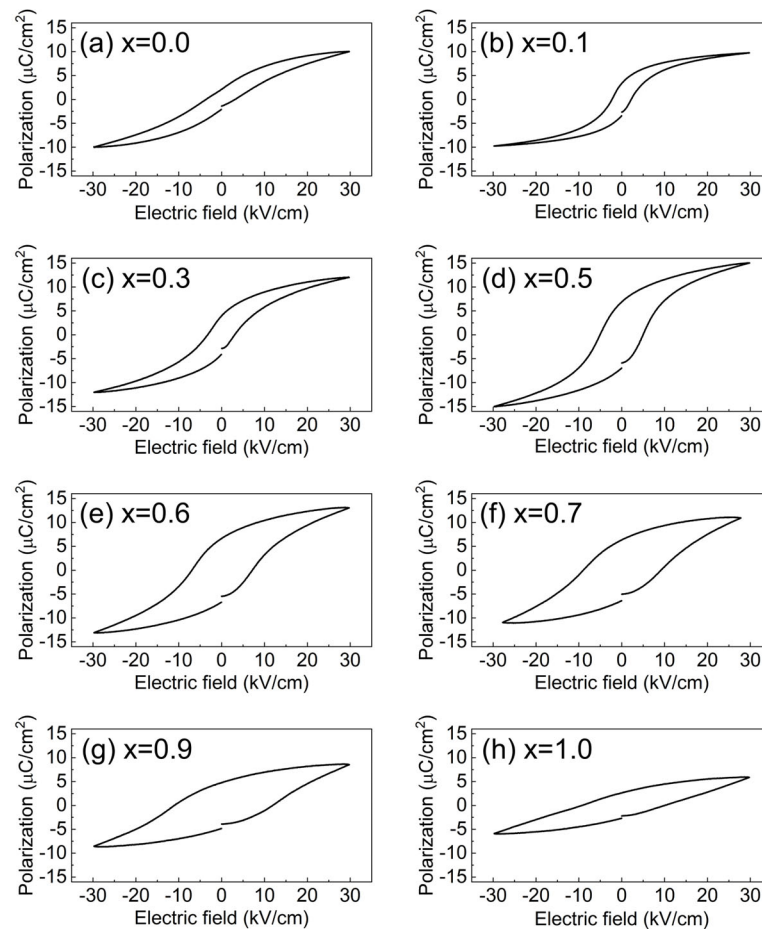
Figure 4. Polarization (P)—electric field (E) hysteresis loops for $BZ_{0.18}T$–$xBP_{0.22}T$: (**a**) 0, (**b**) 0.1, (**c**) 0.3, (**d**) 0.5, (**e**) 0.6, (**f**) 0.7, (**g**) 0.9, and (**h**) 1.0.

The measured piezoelectric coefficients d_{33} of all the samples are shown in Figure 5d. Among all the available compositions, there were two peak values, one at x = 0.1 and the other at x = 0.5. The physical basis of the enhanced piezoelectricity at the MPB is the unique thermodynamic state with low energy barriers between neighboring ferroelectric states [12]. x = 0.5 was the MPB composition of the system, corresponding to the state of two-phase coexistence with a low energy barrier, which endowed it with a relatively low E_C and high polarization, as well as transverse instability under external stimuli [26], thus exhibiting a large d_{33} value (240 pC/N), even exceeding that of the undoped PZT ceramics (160~190 pC/N) [31]. It should be emphasized that two-phase coexistence does not guarantee high piezoelectricity, although enhancement of piezoelectricity is usually observed, as evidenced in BNT-BT materials [10]. The increase in d_{33} of x = 0.5 compared with other off-MPB compositions originates from the thermodynamic feature of MPB, which inherits partly from the triple point where three phases coexist with near-zero energy barriers. Therefore, in principle, the energy barrier of the MPB is lower than that of the polymorphic boundary (PB), and naturally the piezoelectric properties at the MPB are superior to those at the PB [32].

It is interesting that when x = 0.1, neither the end member composition nor the composition at phase boundary also showed a peak value of d_{33} of 186 pC/N, comparable to the performance of undoped PZT ceramic. This should be attributed to the strongest diffuse phase transition behavior detected for the composition x = 0.1 (Table 1), as discussed above. In fact, tuning the normal ferroelectric transition to a diffuse phase transition has been regarded one of the efficient routes to obtain large piezoelectricity [33,34]. Overall,

the composition x = 0.5 exhibited the optimum comprehensive properties regarding the polarization, the coercive field, and the piezoelectricity.
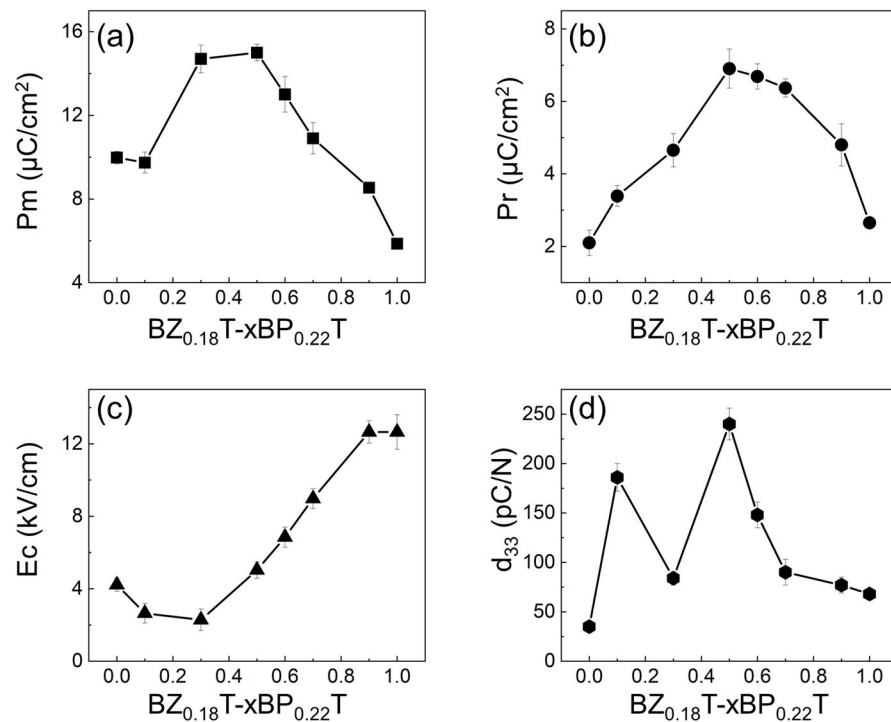

Figure 5. Composition dependence of the maximum polarization Pm (**a**), remnant polarization Pr (**b**), coercive field Ec (**c**), and the piezoelectric coefficient d_{33} (**d**) for $BZ_{0.18}T$–$xBP_{0.22}T$. The lines in the figure are guide for the eye.

Finally, it should be noted that Pb has an increased migration ability during the formation of ferroelectric materials with their content, thus affecting the properties and microstructure of the samples [35–37]. Although the Pb-induced nonstoichiometric and imperfection factors are beyond the scope of the current work, this issue should and will be seriously considered in the future.

4. Conclusions

In conclusion, considering that the worldwide laws and regulations that restrict the content of Pb in functional materials are about to be implemented, and that the currently reported Pb-free piezoelectric materials are far from commercial fabrication, we propose to design low-Pb high-piezoelectric material as an effective alternative. Based on the MPB mechanism, a new MPB-involved system, $BZ_{0.18}T$-$xBP_{0.22}T$, was fabricated. The optimum composition (also the MPB composition), x = 0.5, exhibited a high piezoelectricity of 240 pC/N and a high Tm of 121.1°C. Our result verifies the validity of obtaining good piezoelectricity via fabricating a low-Pb MPB system with one end member of a Pb-free compound and the other end member of a Pb-based compound. We believe that low-Pb piezoelectric materials that can completely replace Pb-rich materials are coming soon.

Institutional Review Board Statement: Not applicable.

Informed Consent Statement: Not applicable.

Data Availability Statement: Not applicable.

Conflicts of Interest: The authors declare no conflict of interest.

References

1. Uchino, K. *Ferroelectric Devices*; Marcel Dekker: New York, NY, USA, 2000; Chapter 7.
2. Jaffe, B.; Cook, W.R.; Jaffe, H. *Piezoelectric Ceramics*; Academic Press: Cambridge, MA, USA, 1971.
3. Choi, S.W.; Shrout, T.R.; Jang, S.J.; Bhalla, A.S. Morphotropic phase boundary in Pb(Mg1/3Nb2/3)O3-PbTiO3 system. *Mater. Lett.* **1989**, *8*, 253–255. [CrossRef]
4. Kuwata, J.; Uchino, K.; Nomura, S. Phase transitions in the Pb(Zn1/3Nb2/3)O3-PbTiO3 system. *Ferroelectrics* **1981**, *37*, 579–582. [CrossRef]
5. Uchino, K. *Piezoelectric Actuators and Ultrasonic Motors*; Springer Science & Business Media: Berlin/Heidelberg, Germany, 1996; Volume 1.
6. Saito, Y.; Takao, H.; Tani, T.; Nonoyama, T.; Takatori, K.; Homma, T.; Nagaya, T.; Nakamura, M. Lead-free piezoceramics. *Nature* **2004**, *432*, 84–87. [CrossRef] [PubMed]
7. Takenaka, T.; Maruyama, K.I.M.K.I.; Sakata, K.S.K. (Bi1/2Na1/2)TiO3-BaTiO3 System for Lead-Free Piezoelectric Ceramics. *Jpn. J. Appl. Phys.* **1991**, *30*, 2236. [CrossRef]
8. Liu, W.; Ren, X. Large Piezoelectric Effect in Pb-Free Ceramics. *Phys. Rev. Lett.* **2009**, *103*, 257602. [CrossRef]
9. Safari, A.; Hejazi, M. Lead-free KNN-based piezoelectric materials. In *Lead-Free Piezoelectrics*; Springer: Berlin/Heidelberg, Germany, 2012; pp. 139–175.
10. Zeng, W.; Zhou, X.; Chen, J.; Liao, J.; Zhou, C.; Cen, Z.; Yang, T.; Yang, H.; Zhou, Q.; Chen, G.; et al. Origin of high piezoelectric activity in perovskite ferroelectric ceramics. *Appl. Phys. Lett.* **2014**, *104*, 242910. [CrossRef]
11. Newnham, R.E. *Properties of Materials: Anisotropy, Symmetry, Structure*; Oxford University Press: Oxford, UK, 2004.
12. Rossetti, J.G.A., Jr.; Khachaturyan, A.G.; Akcay, G.; Ni, Y. Ferroelectric solid solutions with morphotropic boundaries: Vanishing polarization anisotropy, adaptive, polar glass, and two-phase states. *J. Appl. Phys.* **2008**, *103*, 114113. [CrossRef]
13. Zhou, C.; Liu, W.; Xue, D.; Ren, X.; Bao, H.; Gao, J.; Zhang, L. Triple-point-type morphotropic phase boundary based large piezoelectric Pb-free material—Ba(Ti0.8Hf0.2)O3-(Ba0.7Ca0.3)TiO3. *Appl. Phys. Lett.* **2012**, *100*, 222910. [CrossRef]
14. Yu, Z.; Ang, C.; Guo, R.; Bhalla, A.S. Piezoelectric and strain properties of Ba(Ti1-xZrx)O3 ceramics. *J. Appl. Phys.* **2002**, *92*, 1489–1493. [CrossRef]
15. Shirane, G.; Suzuki, K. On the Phase Transition in Barium-Lead Titanate (1). *J. Phys. Soc. Jpn.* **1951**, *6*, 274–278. [CrossRef]
16. Rojac, T.; Drnovsek, S.; Bencan, A.; Malic, B.; Damjanovic, D. Role of charged defects on the electrical and electromechanical properties of rhombohedral Pb(Zr,Ti)O3 with oxygen octahedra tilts. *Phys. Rev. B* **2016**, *93*, 014102. [CrossRef]
17. Zhou, C.; Ke, X.; Yao, Y.; Yang, S.; Ji, Y.; Liu, W.; Yang, Y.; Zhang, L.; Hao, Y.; Ren, S.; et al. Evolution from successive phase transitions to "morphotropic phase boundary" in BaTiO3-based ferroelectrics. *Appl. Phys. Lett.* **2018**, *112*, 182903. [CrossRef]
18. Lines, M.E.; Glass, A.M. *Principles and Applications of Ferroelectrics and Related Materials*; Clarendon: Oxford, UK, 1977.
19. Maiti, T.; Guo, R.; Bhalla, A.S. The evolution of relaxor behavior in Ti4+ doped BaZrO3 ceramics. *J. Appl. Phys.* **2006**, *100*, 114109. [CrossRef]
20. Chattopadhyay, S.; Ayyub, P.; Palkar, V.R.; Multani, M. Size-induced diffuse phase transition in the nanocrystalline ferroelectric PbTiO3. *Phys. Rev. B* **1995**, *52*, 13177–13183. [CrossRef]
21. Jiang, Z.; Yuan, Y.; Yang, H.; Li, E.; Zhang, S. Relaxor regulation and improvement of breakdown strength for Bi0.5Na0.5TiO3-based ceramics by co-doping with Ca and Nb. *Ceram. Int.* **2022**, *48*, 9702–9709. [CrossRef]
22. Wang, J.-J.; Wang, B.; Chen, L.-Q. Understanding, Predicting, and Designing Ferroelectric Domain Structures and Switching Guided by the Phase-Field Method. *Annu. Rev. Mater. Sci.* **2019**, *49*, 127–152. [CrossRef]

23. Chen, Z.; Hong, L.; Wang, F.; Ringer, S.P.; Chen, L.-Q.; Luo, H.; Liao, X. Facilitation of Ferroelectric Switching via Mechanical Manipulation of Hierarchical Nanoscale Domain Structures. *Phys. Rev. Lett.* **2017**, *118*, 017601. [CrossRef]
24. Datta, K.; Margaritescu, I.; Keen, D.A.; Mihailova, B. Stochastic Polarization Instability in PbTiO3. *Phys. Rev. Lett.* **2018**, *121*, 137602. [CrossRef]
25. Heitmann, A.A.; Rossetti, G.A. Thermodynamics of Ferroelectric Solid Solutions with Morphotropic Phase Boundaries. *J. Am. Ceram. Soc.* **2014**, *97*, 1661–1685. [CrossRef]
26. Khachaturyan, A. Ferroelectric solid solutions with morphotropic boundary: Rotational instability of polarization, metastable coexistence of phases and nanodomain adaptive states. *Philos. Mag.* **2010**, *90*, 37–60. [CrossRef]
27. Yuk, S.F.; Pitike, K.C.; Nakhmanson, S.M.; Eisenbach, M.; Li, Y.W.; Cooper, V.R. Towards an accurate description of perovskite ferroelectrics: Exchange and correlation effects. *Sci. Rep.* **2017**, *7*, 43482. [CrossRef] [PubMed]
28. Zhao, L.; Ke, X.; Wang, W.; Zhang, L.; Zhou, C.; Zhou, Z.; Zhang, L.; Ren, X. Electrostrain enhancement at an invisible boundary in a single ferroelectric phase. *Phys. Rev. B* **2017**, *95*, 020101. [CrossRef]
29. Zhang, L.; Zhao, L.; He, L.; Wang, D.; Sun, Y.; Wang, D.; Lou, X.; Zhang, L.; Carpenter, M.A. New Degree of Freedom in Determining Superior Piezoelectricity at the Lead-Free Morphotropic Phase Boundary: The Invisible Ferroelectric Crossover. *ACS Appl. Mater. Interfaces* **2022**, *14*, 1434–1442. [CrossRef]
30. Cohen, R.E.; Krakauer, H. Electronic structure studies of the differences in ferroelectric behavior of BaTiO3 and PbTiO$_3$. *Ferroelectrics* **1992**, *136*, 65–83. [CrossRef]
31. Jaffe, B.; Roth, R.S.; Marzullo, S. Piezoelectric Properties of Lead Zirconate-Lead Titanate Solid-Solution Ceramics. *J. Appl. Phys.* **1954**, *25*, 809–810. [CrossRef]
32. Shrout, T.; Zhang, S. Lead-free piezoelectric ceramics: Alternatives for PZT? *J. Electroceramics* **2007**, *19*, 111–124. [CrossRef]
33. Puli, V.S.; Pradhan, D.K.; Pérez, W.; Katiyar, R.S. Structure, dielectric tunability, thermal stability and diffuse phase transition behavior of lead free BZT–BCT ceramic capacitors. *J. Phys. Chem. Solids* **2013**, *74*, 466–475. [CrossRef]
34. Yao, F.-Z.; Wang, K.; Jo, W.; Webber, K.G.; Comyn, T.P.; Ding, J.-X.; Xu, B.; Cheng, L.-Q.; Zheng, M.-P.; Hou, Y.-D.; et al. Diffused Phase Transition Boosts Thermal Stability of High-Performance Lead-Free Piezoelectrics. *Adv. Funct. Mater.* **2016**, *26*, 1217–1224. [CrossRef]
35. Mukhin, N.V. Diffusion model of intrinsic defects in lead zirconate titanate films on heat treatment in air. *Glas. Phys. Chem.* **2014**, *40*, 238–242. [CrossRef]
36. Mangum, J.S.; Podowitz-Thomas, S.; Nikkel, J.; Zhou, C.; Jones, J.L. Investigating Pb diffusion across buried interfaces in Pb(Zr0.2Ti0.8)O3 thin films via time-of-flight secondary ion mass spectrometry depth profiling. *Surf. Interface Anal.* **2017**, *49*, 973–977. [CrossRef]
37. Mukhin, N.; Chigirev, D.; Bakhchova, L.; Tumarkin, A. Microstructure and Properties of PZT Films with Different PbO Content—Ionic Mechanism of Built-In Fields Formation. *Materials* **2019**, *12*, 2926. [CrossRef] [PubMed]